

# A Coupled Lateral/Directional Flight Dynamics and Structural Model for Flight Control Applications

Ondrej Juhasz\*

*San Jose State University Research Foundation, Moffett Field, CA*

Mark B. Tischler†

*U.S. Army Aviation Development Directorate-AFDD, Moffett Field, CA*

Steven G. Hagerott,‡ David Staples,§ and Javier Fuentealba ¶

*Cessna Aircraft Company, Wichita, KS*

A lateral/directional flight dynamics model which includes airframe flexibility is developed in the frequency domain using system-identification methods. At low frequency, the identified model tracks a rigid-body (static-elastic) model. At higher frequencies, the model tracks a finite-element NASTRAN structural model. The identification technique is implemented on a mid-sized business jet to obtain a state-space representation of the aircraft equations of motion including two structural modes. Low frequency structural modes and their associated notch filters impact the flight control frequency range of interest. For a high bandwidth control system, this frequency range may extend up to 30 rad/sec. These modes must be accounted for by the control system designer to ensure aircraft stability is retained when a control system is implemented to help avoid aeroservoelastic coupling. A control system is developed and notch filters are selected for the developed coupled aircraft model to demonstrate the importance of including the structural modes in the design process.

## Nomenclature

$\beta$	Sideslip angle
$\zeta_{dr}$	Dutch-roll damping ratio
$\zeta_{strn}$	Damping ratio of structural mode $n$
$\eta_{\delta n}$	Control derivative for structural mode $n$
$\eta_{strn}, \dot{\eta}_{strn}, \ddot{\eta}_{strn}$	Displacement, rate, acceleration for structural mode $n$
$\eta_{vn}, \eta_{pn}, \eta_{rn}$	Rigid-body coupling terms for structural mode $n$
$\phi$	Roll attitude at aircraft CG
$\Phi_{yn}$	Influence coefficient at sensor $y$ for structural mode $n$
$\omega_{dr}$	Dutch-roll frequency
$\omega_{strn}$	Frequency of structural mode $n$
$p$	Roll rate at aircraft CG
$r$	Yaw rate at aircraft CG
$T_s$	Spiral mode time constant
$T_r$	Roll mode time constant
$v$	Lateral velocity at aircraft CG
$y_w$	Wing semi-span

---

\*Research Associate, Member AIAA

†Flight Control Technology Group Leader, Senior Scientist, Associate Fellow AIAA.

‡Senior Engineer Specialist, Senior Member AIAA.

§Senior Engineer Specialist, Member AIAA.

¶Engineer Specialist, Member AIAA

## I. Introduction

MODERN aircraft designs incorporate weight saving features which often lead to low frequency structural modes. As these structural modes decrease in frequency, they begin to impact the frequency range of interest for flight control. This frequency range generally extends from 1/5 to 5 times the crossover frequency and may approach 30 rad/sec for high bandwidth control systems.<sup>1</sup> It is critical that the flight control system designer be aware of and account for these modes during the control system design process. The presence of these modes can have a significant impact on both aircraft stability margins and closed loop performance.

In-flight frequency sweeps have been used to identify flexible aircraft models.<sup>2,3,4,1</sup> Time domain identification has also been performed on flexible wing gliders.<sup>5,6</sup> However, flight data is not available during the aircraft design process so predictive models must be used. During the initial stages of aircraft design flight dynamics models are generally available for control system development and finite-element models are available to assess the structural design. Ground vibration test models may also be used if a detailed structural model is not available. The flight dynamics and structural models must be combined in order to obtain an integrated high-fidelity linear model valid over a broad frequency range. The identified structural model can then be validated directly against flight data when the aircraft enters flight testing.

This paper presents the coupling of a rigid-body aircraft model with a finite-element NASTRAN structural model using system identification methods. The resulting *hybrid-flexible* model accurately includes flight dynamics and the first two structural modes up to 30 rad/sec. Higher frequency modes are still critical from a flutter perspective, but have minimal impact on the flight dynamics characteristics of an aircraft. These modes have sufficient frequency separation from the flight control system such that the coupling is negligible. The rigid-body aircraft model is derived from wind-tunnel data and known mass properties to give an accurate representation of the low frequency dynamics. The finite-element model is not accurate at low frequency, but captures the structural modes and sensor responses due to structural motion.

The combined hybrid-flexible model can be used for optimal notch-filter design or for active control of structural modes. If a state-space model including structural modes is available during the design process, notch filters may be configured independently for each mode's worst case excitation, minimizing the associated phase degradation at lower frequencies. Stability requirements at and above structural frequencies may be included and met during the initial design stage, reducing the iterative "tuning" associated with a flight control system once a rigid-body design is complete. Notch filters for modes higher than 30 rad/sec have a large frequency separation from, and may be sized without impact on, the flight dynamic characteristics of the aircraft. The identification procedure can also be used to analyze the impact of moving sensor locations in the aircraft.

The objective of this paper is to show the development of a business jet flight dynamics model that is accurate over a broad frequency range and includes effects of structural modes below 30 rad/sec. The model is determined using system identification techniques in the frequency domain. A comprehensive set of input/output pairs are used to ensure the model is accurate for different responses at varying sensor locations. A representative control system is also developed that compares the stability and closed-loop response of the rigid-body and flexible models to demonstrate the importance of structural modes in the design process. The frequency scales are suppressed throughout the paper due to the proprietary nature of the data.

## II. Aircraft Description

The example aircraft used herein is a mid-sized business jet. The aircraft has a maximum cruise speed of approximately 500 KTAS, and a seating capacity of eight passengers. The *nominal* model developed is for a lightly loaded Mach 0.8 cruise flight condition. Along with a nominal loading and speed case, an *off-nominal* case is also considered. The structural responses for the nominal and off-nominal models are compared with responses over the entire flight envelope in Fig. 1. These cases help ensure the model structure and identification methods are adequate over the entirety of the flight envelope. The careful selection of the nominal and off-nominal cases to span the flight envelope can significantly reduce the number of flight conditions that need to be verified to meet stability requirements. There is currently a large array of dynamic pressure, Mach number, and loading configurations that are tested to ensure stability. The reduction of this

array of responses could result in time savings during the control design process and flight test.

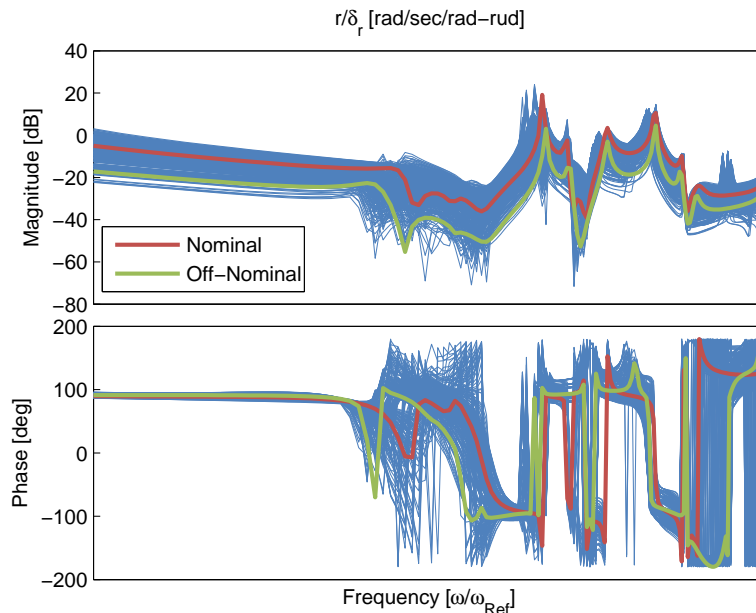


Figure 1. Yaw response comparisons at structural frequencies over all flight conditions

### III. Background on Modeling and Control of Flexible Aircraft

*Passive control* of structural modes through the use of notch filters is generally adequate to reduce structural excitation and ensure stability of structural modes. Nearly all modern aircraft include notch filters on the dominant structural modes for each axis. Notch filters on structural modes with low frequencies may reduce stability margins at the flight dynamics frequencies.

Structural modes may also be *actively controlled* provided the requisite mode sensing is available. Modern large transport aircraft include active structural mode control for ride quality improvements in turbulence.<sup>3,7,8</sup> The models used for the control synthesis were identified from flight data. One of the control systems utilizes LQR type gain determination that aims to minimize structural acceleration at various sensor locations.<sup>3</sup> In Ref. 9, an active structural control system was developed for a large flexible tiltrotor aircraft that minimized structural motion in turbulence and also met handling quality and stability requirements. Reducing structural motion at the pilot station was accomplished on the B-1 bomber using structural control vanes.<sup>10</sup> The structural model for this aircraft was identified from flight test and combined with a flight dynamics model to give an accurate representation of aircraft dynamics.

Many forms of flight dynamics models that include aircraft flexibility have been developed. The largest subset of these models are referred to as *mean-axis* models and assume a rigid-aircraft that is augmented by structural modes.<sup>11,12,13</sup> The structural modes must be known *a-priori* and are fully coupled with the rigid-body degrees of freedom.

*Multibody* models have also been developed.<sup>14</sup> Here, structural, inertial, and aerodynamic forcing from each individual component of the aircraft are summed together, one body at a time. The resulting system is fully coupled and the states represent motion of individual components of the aircraft. These physics-based models have large development costs since the comprehensive solution contains structural, aerodynamic and inertial contributions over a broad frequency range.

Simpler models may be developed under the assumption of one-way coupling between the rigid-body and structural states.<sup>15</sup> The identification of a large flexible transport and the original development of the model used in this paper also employed on-way coupling.<sup>4</sup> This *hybrid-flexible* model structure, later refined by Tischler,<sup>1</sup> is a one-way coupled representation that captures the structural dynamics in a simplified form that is well suited to system-identification of models from flight data and finite-element modeling data. Physics-based mean-axis and multibody models contain many highly correlated parameters, which makes

system identification impractical. The one-way coupled hybrid-flexible models become more accurate as the separation between the rigid-body and structural states increases. The hybrid-flexible model structure is expected to give good results if the frequencies of the lowest structural modes are at least five times greater than the highest rigid-body modes:<sup>1</sup>

$$\frac{\omega_{\min \text{ structural}}}{\omega_{\max \text{ rigid-body}}} \geq 5 \quad (1)$$

This requirement is met for many practical aircraft applications.<sup>1</sup> The multibody or mean-axis models may provide higher fidelity, but for flight control applications, the hybrid-flexible model captures the key dynamics of the responses and is simpler to identify.

The final and simplest model structure is a *decoupled* structure, where the rigid-body and structural dynamics are independent of each other and the structural contribution to motion at a sensor is introduced in the outputs.<sup>3</sup> Decoupled models have been shown to be inadequate in several practical applications.<sup>16,1</sup> Detailed descriptions and comparisons of these flight dynamics models are given by Juhasz<sup>16</sup> and Tischler.<sup>1</sup>

#### IV. Model Formulation Strategy

The model formulation process uses system identification methods to determine a hybrid-flexible flight dynamics model. Table 1 gives the frequency separation and nomenclature for the structural and rigid-body modes. For the example aircraft used herein, the guideline given by Eqn. (1) is nearly met for the lowest frequency structural mode. Therefore, the hybrid-flexible model should be suitable for the identification procedure.

Table 1. Aircraft and structural modal frequencies

Mode	Damping Ratio $\zeta$	Frequency $\omega$
Spiral	-	$1/T_s$
Dutch-Roll	$\zeta_{dr}$	$\omega_{dr}$
Roll	-	$1/T_r$
First Structural	$\zeta_{str1}$	$\omega_{str1} \times T_r = 4.5$

The hybrid-flexible model structure is developed in state-space form:

$$\{\dot{x}\} = [A] \{x\} + [B] \{u\} \quad (2)$$

$$(3)$$

The state vector can be reorganized into parts containing rigid-body terms and parts containing structural flexibility terms.

$$\{x\} = \begin{Bmatrix} x_{rb} \\ x_{str} \end{Bmatrix} \quad (4)$$

The hybrid-flexible stability derivative matrix is:

$$A = \left[ \begin{array}{c|ccc} \text{Static - Elastic} & 0 & \dots & 0 \\ \text{Stability} & \vdots & 0 & \vdots \\ \text{Derivatives} & 0 & \dots & 0 \\ \text{-----} & + & \text{-----} & \\ \text{Rigid - Body} & | & \text{Structural} & \\ \text{Coupling} & | & \text{Flexibility} & \\ \text{Terms} & | & \text{Modes} & \end{array} \right] \quad (5)$$

The control derivative matrix is:

$$B = \begin{bmatrix} \text{Static – Elastic} \\ \text{Control} \\ \text{Derivatives} \\ \text{-----} \\ \text{Structural} \\ \text{Mode Control} \\ \text{Derivatives} \end{bmatrix} \quad (6)$$

This model retains one-way forcing from the rigid-body states into the structural states. These terms are referred to as *rigid-body coupling* terms and appear in the off-diagonal of the state matrix. Forcing effects of the structural states onto the rigid-body states are considered quasi-static and result in the use of the *static-elastic* model for the rigid-body states, and so the upper-right quadrant of the  $[A]$  matrix is zero. The static-elastic derivatives retain static structural deflection effects on the rigid-body motion of the aircraft. For example, the influence of trim structural deflections in the calculation of the stability and control derivatives may include symmetric wing bending due to steady-state loads or loss of aileron effectiveness due to wing torsional bending for aileron inputs.

The output vector is also written in standard state-space form as:

$$\{y\} = [C] \{x\} + [D] \{u\}$$

The output matrix contains the influence coefficients on the structural states:

$$C = \begin{bmatrix} \text{Static – Elastic} & | & \text{Influence} \\ \text{Outputs} & | & \text{Coefficients} \end{bmatrix} \quad (7)$$

Structural contributions at the sensor locations are introduced in the output equations through the use of *influence coefficients* ( $\Phi$ ), which add local displacement information due to structural motion to the output equation to the static-elastic ( $_{se}$ ) output. Every sensor has influence coefficients available for each mode. The larger the influence coefficient, the larger the impact of a structural mode in the response at that sensor location.

An example flexible roll rate measurement would be as follows:

$$p = p_{se} + \Phi_{p1} \dot{\eta}_{str1} + \dots + \Phi_{pn} \dot{\eta}_{strn} \quad (8)$$

## V. Static-Elastic and Structural Models

The static-elastic and NASTRAN structural models that are integrated into the identified hybrid-flexible model are described herein in greater detail. The static-elastic and flexible models are compared to ensure they give similar mid frequency results (frequencies between the low frequency rigid-body modes and the first structural mode).

### V.A. Static-Elastic Model

The static-elastic models were derived analytically based on a standard 3-degree-of-freedom lateral/directional linear model structure.<sup>17</sup> The given model structure has a general formulation and is valid for any aircraft. The specific source data for the linear model of the aircraft presented in this study include: wind tunnel derived stability and control derivatives, DATCOM estimated rate derivatives, and design aircraft weight and inertias. Control power “knockdowns” were applied to the roll rate ( $L_p$ ) and aileron terms, based on steady-state aeroservoelastic estimates. These knockdowns account for the effect of steady-state structural deflections on the rigid-body stability and control derivatives and give the static-elastic derivatives. No control power knockdown terms were applied to the yaw rate or rudder derivatives.

## V.B. Structural Model

The NASTRAN aeroelastic model is of a type commonly used for flutter and dynamic loads analysis.<sup>18</sup> As a “stick-type” dynamic model, it is based on massless elastic bars to which distributed, lumped mass properties and piece-wise constant stiffness are assigned. Idealized spring elements are employed to model control surface rotational modes and local compliances between major structural components. Mass and stiffness properties are estimated by proprietary methods used in the advanced-design phase of project development. Variable mass items simulate different fuel and payload configurations. The complete model for this study has 1067 nodes and 2051 elements.

The 6-degree-of-freedom simulation normally yields six rigid-body modes and flexible structural modes up to 50Hz. For the present work, which only contains lateral-directional degrees of freedom, the three longitudinal rigid-body modes (pitch/plunge/fore-aft) were deleted from the solution, though all of the flexible structural modes were retained. NASTRAN multi-point constraint elements are used to coordinate left-right control surface rotational modes, so that both symmetric and anti-symmetric aileron and elevator modes are provided in all executions.

Unsteady aerodynamics are based on the Doublet-Lattice Method.<sup>19,20</sup> Unsteady aerodynamics are implemented in NASTRAN Solutions 145 (Flutter) and 146 (Dynamic Aeroelasticity). This procedure represents a planar lifting surface as a grid of trapezoidal lifting elements, or “boxes,” with velocity distributions generated by doublet singularities. The current model has 3316 aerodynamic box elements. These aerodynamic elements are splined to the structural nodes so that aerodynamic forces are applied to the structure and structural motion in turn deflects the aerodynamic boxes. In the present model, the fuselage, engine nacelles, and pylons have no aerodynamic elements applied, but in a fully-developed model such elements would be used to help tune the zero-frequency steady-state aerodynamics to match the quasi-steady stability derivatives. In the present case, this tuning was not undertaken.

## V.C. Comparisons of Static-Elastic and Structural Models

The static-elastic model is available in state-space form. The associated conventional lateral/directional modes are obtained from an eigenanalysis of the stability derivative matrix and the aircraft is constrained to move within the included three degrees of freedom. Control systems can be developed for this type of model and they can be easily used in simulations. The finite-element NASTRAN model is also in modal form in that the airframe is only allowed to bend through retained mode shapes at known frequencies. Measurements of the structural motion are given by frequency responses at known locations throughout the aircraft which give magnitude and phase information at the location to an input. The work presented here forms a hybrid-flexible state-space model from the combination of the static-elastic and NASTRAN structural models.

In order to successfully identify the aircraft dynamics, the static-elastic and finite-element models must be consistent with each other. Input and measurement quantities must be in the same axes system and be defined the same way. For example, in the static-elastic model aileron inputs are positive for right-wing trailing edge down deflections. The total antisymmetric aileron deflection is a difference between the right and left aileron:

$$\delta_{\text{ail}} = \delta_{\text{ail } w_r} - \delta_{\text{ail } w_l} \quad (9)$$

The NASTRAN finite-element data is converted to the stability axes to match the static-elastic model conventions. Even though the models generally match very well without additional scaling, small scaling allowances applied to the NASTRAN data ensure the models “line up” well at mid frequencies. The identification process ensures that at low frequencies the identified model matches the static-elastic response and at high frequencies it matches the NASTRAN data. Therefore, it is important that there is a smooth transition and that there are no discontinuities from one data set to the other. The scale factors replace the zero-frequency tuning of the NASTRAN model from Sec. V.B and can be attributed to differences in aerodynamic modeling between the static-elastic and NASTRAN models.

Figure 2(a) shows the roll rate response to aileron inputs of the static-elastic and NASTRAN models, and indicates that only a very small correction is needed. Wing tip differenced vertical acceleration (Fig. 2(b)) is obtained by subtracting the left wing’s vertical response from the right wing’s, and is compared to a calculated acceleration response taken by multiplying the static-elastic CG roll acceleration by the semi-span and dividing by gravity. As with the roll rate, only a small correction is needed for the NASTRAN

data.

$$\Delta n_{zw} = \frac{n_{zw_r} - n_{zw_l}}{2} \quad (10)$$

$$= \frac{y_w \dot{\rho}_{se}}{g} \quad (11)$$

Figure 3 shows a similar set of plots for rudder inputs. Yaw rate and differential fore/aft wing tip acceleration are compared for the static-elastic and NASTRAN models. No scaling was necessary for a majority of the NASTRAN rudder responses.

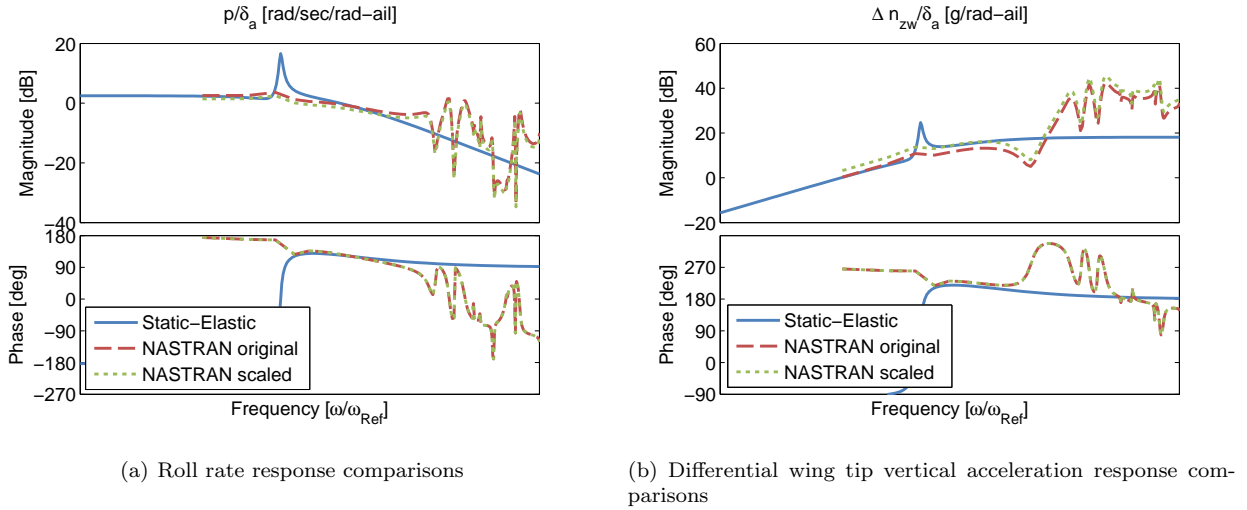


Figure 2. Comparisons of NASTRAN and static-elastic responses to aileron inputs

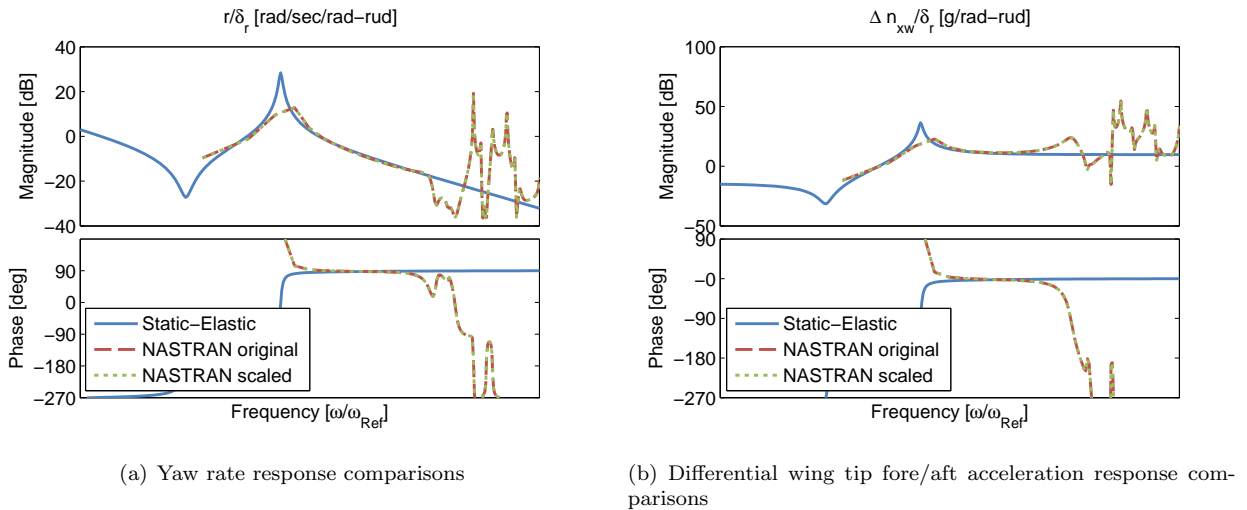


Figure 3. Comparisons of NASTRAN and static-elastic responses to rudder inputs

The frequencies ranges where the different models are accurate is quite obvious from Figs. 2 and 3. There is minimal content at low frequencies in the NASTRAN responses. Here, the static-elastic responses show dutch-roll and roll subsidence dynamics well.

At higher frequencies, the NASTRAN model shows the complex structural dynamics while the static-elastic model is at the response asymptotic value. The first structural mode occurs around 20 rad/sec and is depicted in Fig. 4(a). This mode couples roll and yaw motion at the CG, meaning vertical and fore/aft wing tip acceleration is present. The second structural mode (Fig. 4(b)) occurs around 26 rad/sec and contains predominantly roll and antisymmetric wing bending deflections.

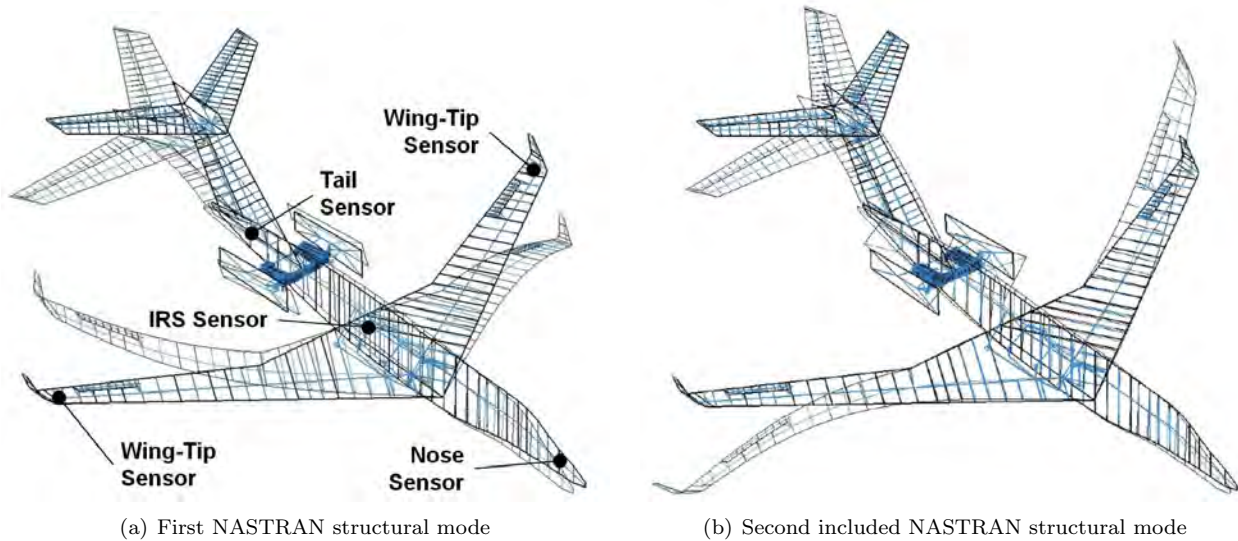


Figure 4. NASTRAN structural modes included in identification process

## VI. Identification of a Hybrid-Flexible Lateral/Directional Model for the Nominal Flight Condition

The coupled hybrid-flexible model for the nominal loading and speed case is identified using the frequency domain system identification tool CIFER<sup>®</sup>.<sup>1</sup> The identification achieves the best possible match of the many NASTRAN and static-elastic frequency responses for both aileron and rudder excitation. The frequency response functions generated from the NASTRAN model are listed in Table 2 and the associated sensor locations are also shown in Fig. 4(a).

Table 2. Sensor locations used in identification process

Name	Response(s) used in identification procedure
IRS	Location of aircraft's inertial reference system (IRS) sensors mounted near the aft wing spar. Contains angular rate and linear acceleration measurements
Nose	Lateral linear acceleration at nose
Tail	Lateral linear acceleration at tail
Wing Tip ( $\Delta n_w$ )	Differential vertical and fore/aft wing tip linear acceleration

The CIFER<sup>®</sup> identification method minimizes a coherence weighted cost function based on the error between the frequency responses of the identified model and those of the NASTRAN and static-elastic models. In the current application the responses are all from simulation, so the coherence is set to unity. The free parameters in the state-space model structure of Eqns. (5)-(7) serve as the unknowns in the optimization process.

A numerical sensitivity analysis is conducted within CIFER<sup>®</sup> to determine the Insensitivity and Cramer-Rao values of parameters.<sup>1</sup> The insensitivity of a parameter is the measure of that parameter's importance in the chosen model structure. Parameters with high insensitivity may be set to zero and removed from the model structure without any effect on the accuracy of the solution. The goal is to determine a model structure where parameter insensitivities are less than 10%.<sup>1</sup>

$$I_i \leq 10\% \quad (12)$$

If several insensitivities are slightly higher than 10%, there is no expected loss in the reliability of the solution.

In CIFER<sup>®</sup>, the Cramer-Rao bounds are a reliable measure of  $1\sigma$  parameter accuracy. Parameters with low Cramer-Rao bounds are identified with great confidence and are key to the solution accuracy.

Parameters with high Cramer-Rao bounds are correlated with other parameters in the identification. If good initial guesses are available, these correlated parameters may be fixed at the known values. Otherwise, these parameters may be set to zero and dropped with no loss of modeling accuracy. The parameters are identified very well if the Cramer-Rao bounds are less than 20%.<sup>1</sup>

$$CR_i \leq 20\% \quad (13)$$

If several Cramer-Rao bounds are slightly higher than 20%, there is no expected loss in the reliability of the solution.

An example lateral/directional hybrid-flexible model including one structural mode has the following form from Eqns. (5)-(7):

$$x = \left\{ v \quad p \quad r \quad \phi \quad \dot{\eta} \quad \eta \right\}^T \quad (14)$$

$$y_{\text{sens}} = \left\{ p_{\text{sens}} \quad r_{\text{sens}} \right\}^T \quad (15)$$

$$A = \left[ \begin{array}{cccc|cc} Yv & Yp & Yr & g & 0 & 0 \\ Lv & Lp & Lr & 0 & 0 & 0 \\ Nv & Np & Nr & 0 & 0 & 0 \\ 0 & 1 & 0 & 0 & 0 & 0 \\ \hline \eta_{v1} & \eta_{p1} & \eta_{r1} & 0 & -2\zeta_{\text{str}1}\omega_{\text{str}1} & -\omega_{\text{str}1}^2 \\ 0 & 0 & 0 & 0 & 1 & 0 \end{array} \right] \quad (16)$$

$$B = \left[ \begin{array}{cc} Y_{\delta_{\text{ail}}} & Y_{\delta_{\text{rud}}} \\ L_{\delta_{\text{ail}}} & L_{\delta_{\text{rud}}} \\ N_{\delta_{\text{ail}}} & N_{\delta_{\text{rud}}} \\ 0 & 0 \\ \hline \eta_{\delta_{\text{ail}1}} & \eta_{\delta_{\text{rud}1}} \\ 0 & 0 \end{array} \right] \quad (17)$$

For the sample roll and yaw rate outputs at a given sensor location, the influence coefficients are implemented as:

$$C = \left[ \begin{array}{cccc|cc} 0 & 1 & 0 & 0 & \Phi_{p_{\text{sens}1}} & 0 \\ 0 & 0 & 1 & 0 & \Phi_{r_{\text{sens}1}} & 0 \end{array} \right] \quad (18)$$

Since the static-elastic rigid-body model is known, it is held fixed in the upper left quadrant. The static-elastic control derivatives are also held fixed. Initial values for the structural frequency can be well estimated from the NASTRAN responses (Fig. 1) and an initial value of structural damping can be set to a minimal value (e.g.  $\zeta = 0.02$ ). These are placed in the lower-right quadrant of the stability derivative matrix. The rigid-body coupling terms, influence coefficients, and structural control derivatives are not known, so they are initialized to be zero. A model including a single structural mode is identified first. Once this model is determined, a model including two modes is identified.

## VI.A. Identification of a Hybrid-Flexible Model Including the First Structural Mode

Table 3 summarizes the frequency response pairs used in the identification and the frequency range of the fit for each response. The maximum frequency for identification was chosen to be just above the first structural mode frequency. Including frequencies much above the first mode would allow higher frequency structural

modes to impact the solution, degrading the results. Following Ref. 1, the frequency ranges of the responses must satisfy the guideline:

$$\frac{\omega_{max}}{\omega_{min}} \geq 2 \quad (19)$$

It is seen in Table 3 that this guidelines is met. Since the static-elastic control and stability derivatives are fixed, the low frequency dynamics of the identified model are equal to the static-elastic model. Therefore, low frequency (quasi-static) responses do not need to be included in the identification process.

**Table 3. Structural mode responses and frequency ranges for model identification including only the first structural mode**

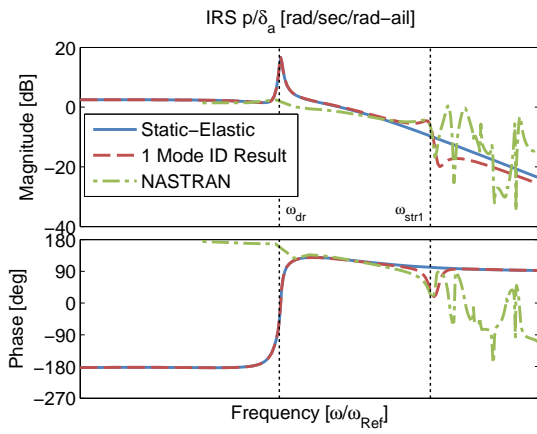
Output	Input	Response Name	$\omega_{min}$	$\omega_{max}$
$p_{IRS}$	Aileron	$pIR/ail$	10	21
$r_{IRS}$	Aileron	$rIR/ail$	10	21
$n_{y_{IRS}}$	Aileron	$ayIR/ail$	10	21
$n_{y_{Nose}}$	Aileron	$ayNs/ail$	10	21
$\Delta n_{zW}^*$	Aileron	$azDW/ail$	10	21
$r_{IRS}$	Rudder	$rIR/rud$	10	21
$n_{y_{IRS}}$	Rudder	$ayIR/rud$	10	21
$n_{y_{Nose}}$	Rudder	$ayNs/rud$	10	21
$n_{y_{Tail}}$	Rudder	$ayTl/rud$	10	21
$\Delta n_{zW}^*$	Rudder	$azDW/rud$	10	21
$\Delta n_{xW}^*$	Rudder	$azDW/rud$	10	21

\* Created from differencing individual wing accelerometer measurement, Eqn. (10)

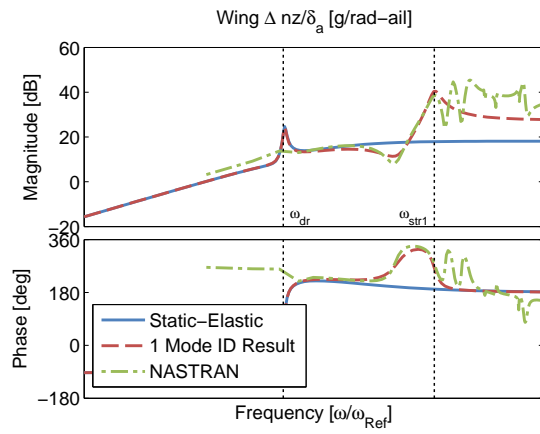
The identified responses are compared with the static-elastic and NASTRAN responses in Fig. 5. A more complete set of responses, including additional off-axis responses, will be shown for the identification including two structural modes. The identified model, combining both static-elastic and NASTRAN dynamics, captures the dynamics well up to the first structural mode for all the responses. Since the static-elastic derivatives were fixed in the identification, the low frequency rigid-body dynamics match exactly with the static-elastic model. Both aileron responses show strong influence of the the first structural mode (Figs. 5(a) and 5(b)). The mode also shows up well in the nose (Fig. 5(e)) and wing tip (Fig. 5(f)) responses to rudder as these sensor locations have large modal deflections. The structural mode does not have much influence in the yaw rate response at the IRS sensor, as can be seen in Fig. 5(c). This is because the IRS sensor is located on a angular node for the mode (see Fig. 4(a)).

The cost functions for the final design are given in Table 4. The fairly limited frequency range of interest for the identification leads to an amplification of the costs for some of the structural responses, although the average cost of  $J_{ave} = 73$  well meets the guideline for good modeling accuracy:  $J_{ave} < 100$ ,<sup>1</sup> consistent with the good agreement seen in the frequency response plots.

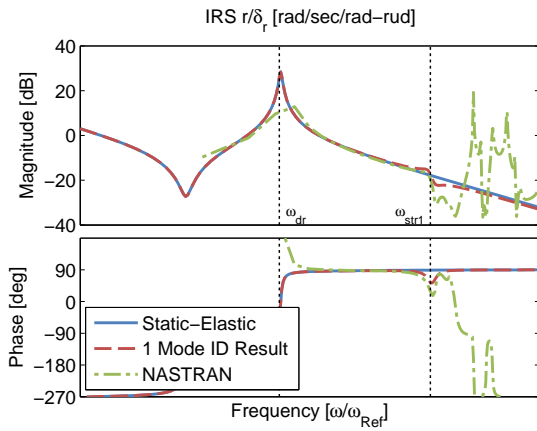
The final identified parameter values are suppressed due to the proprietary nature of the data, but Cramer-Rao and insensitivity values for each parameter are shown in Table 5. The results are well within the guidelines given by Eqns. 12 and 13, indicating a reliable model. This table shows two of the rigid-body coupling terms ( $\eta_{v1}$  and  $\eta_{p1}$ ) were eliminated in the identification. The first structural mode is predominantly excited by yaw rate, therefore the lateral velocity and roll rigid-body coupling terms were not well identifiable. The influence coefficients ( $\Phi$ ) are left free. Only one control derivative was left free. For a single structural mode, the structural control derivatives are fully correlated with the influence coefficients. The response at the structural frequencies may be changed either by altering the control derivative (overall structural excitation) or the influence coefficient for a response (magnitude of structural response at sensor). Since the first structural mode is mainly excited by the rudder, the aileron control derivative ( $\eta_{\delta_{ail1}}$ ) was fixed at unity. The influence coefficients are then set by the aileron response and the correlation problem was eliminated.



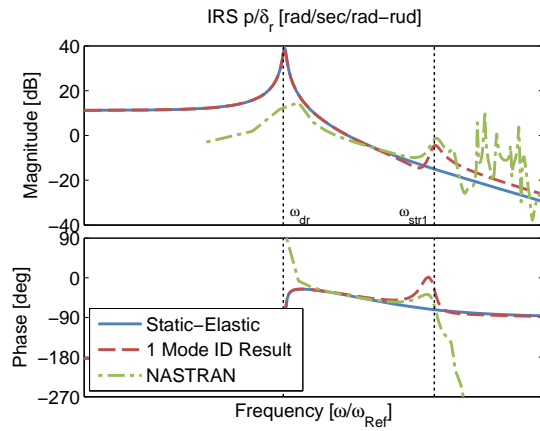
(a) Roll rate response to aileron at the IRS sensor



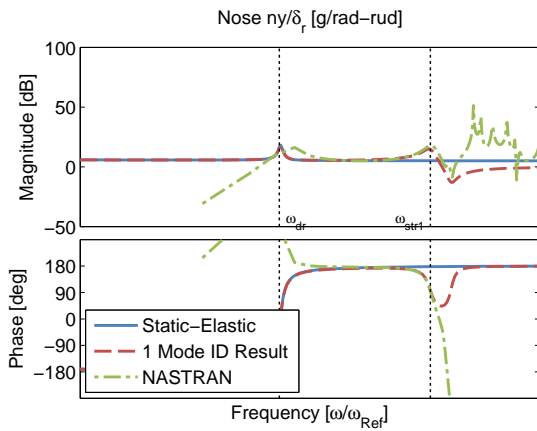
(b) Differential wing tip vertical acceleration response to aileron



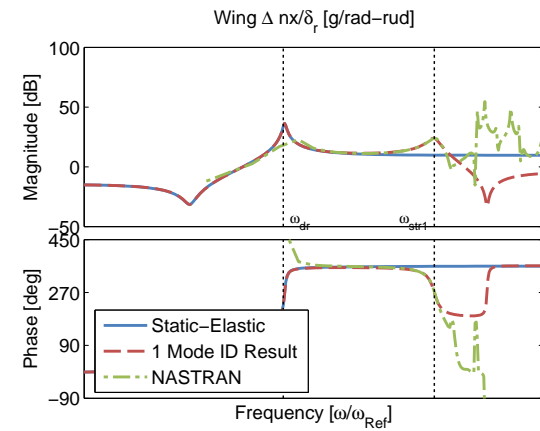
(c) Yaw rate response to rudder at the IRS sensor



(d) Roll rate response to rudder at the IRS sensor



(e) Lateral acceleration response to rudder at the nose



(f) Differential wing tip fore/aft acceleration response to rudder

Figure 5. Identified model results including one structural mode

Table 4. Identification Costs for First Structural Mode Model

Response	Cost
$pIR/ail$	79.07
$rIR/ail$	148.5
$nyIR/ail$	18.39
$nyNs/ail$	79.9
$nzDW/ail$	124.1
$rIR/rud$	149.9
$nyIR/rud$	12.81
$nyNs/rud$	72.75
$nyTl/rud$	62.46
$nzDW/rud$	47.52
$nxDW/rud$	3.903
$J_{ave}$	72.66

Table 5. Cramer-Rao and Insensitivity Values for Identification of First Structural Mode Model

Engineering Symbol	CR (%)	Insens. (%)
$\eta_{v1}$ <sup>b</sup>	—	—
$\eta_{p1}$ <sup>b</sup>	—	—
$\eta_{r1}$	14.14	6.044
$2\zeta_{str1}\omega_{str1}$	3.665	1.325
$\omega_{str1}^2$	0.4934	0.2025
$\eta_{\delta_{ail1}}$ <sup>a</sup>	—	—
$\eta_{\delta_{rud1}}$	3.635	1.293
$\Phi_{pIRS1}$	7.238	3.43
$\Phi_{rIRS1}$	5.682	2.643
$\Phi_{nyIRS1}$	4.134	1.794
$\Phi_{nyNose1}$	4.108	1.811
$\Phi_{nyTail1}$	21.34	10.47
$\Phi_{\Delta n_{zw}1}$	2.592	1.088
$\Phi_{\Delta n_{xw}1}$	6.767	2.802

<sup>a</sup> Fixed parameter

<sup>b</sup> Eliminated parameter

## VI.B. Identification of a Hybrid-Flexible Model Including Two Structural Modes

The second identified structural mode, Fig. 4(b), is a wing antisymmetric wing bending mode excited mainly by the ailerons.

The inclusion of the second mode is identical to that of the first structural mode. Two additional states are added to the state vector. Another set of rigid-body coupling terms and influence coefficients are also added. The identification process was initialized using the results from the single structural mode model. These parameters were first fixed at their original value and the parameters of the second structural mode were optimized. Once the solution converges to an initial set of parameters for the second mode, the first mode's parameters are also freed and the entire model is reconverged.

The frequency response pairs are summarized in Table 6. The frequency ranges presented for the aileron inputs include both the first and second structural modes, increasing the frequency range of the model to well above the guideline in Eqn. (19). The frequency ranges of identification for the rudder responses remain limited to the first structural mode (about the same as Table 3) since the second mode has little influence on the responses.

**Table 6. Structural mode responses and frequency ranges for model identification including two structural modes**

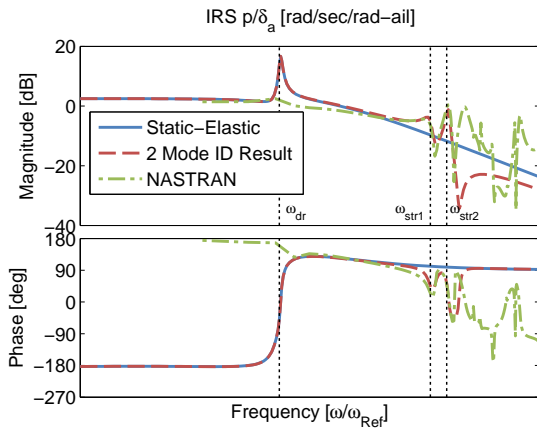
Output	Input	Response Name	$\omega_{min}$	$\omega_{max}$
$p_{IRS}$	Aileron	$pIR/ail$	10	28
$n_{y_{IRS}}$	Aileron	$ayIR/ail$	10	28
$n_{y_{Nose}}$	Aileron	$ayNs/ail$	10	28
$\Delta n_{zW}^*$	Aileron	$azDW/ail$	10	28
$r_{IRS}$	Rudder	$rIR/rud$	10	22
$n_{y_{IRS}}$	Rudder	$ayIR/rud$	10	22
$n_{y_{Nose}}$	Rudder	$ayNs/rud$	10	22
$\Delta n_{zW}^*$	Rudder	$azDW/rud$	10	22
$\Delta n_{xW}^*$	Rudder	$azDW/rud$	10	22

\* Created from differencing individual wing accelerometer measurement, Eqn. (10)

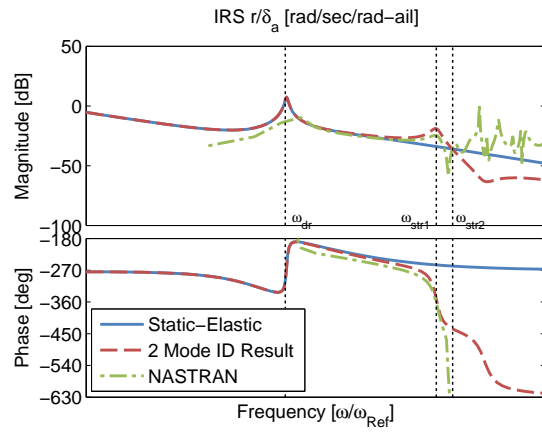
The aileron responses including the two identified structural modes are shown in Fig. 6. Both structural modes are well identified in the roll rate and differential vertical wing tip acceleration responses, Figs. 6(a) and 6(e), respectively. These are the dominant responses in the roll axis. Both modes are also well identified in the other responses. The rudder responses are shown in Fig. 7. The lack of excitation of the second mode by the rudder is apparent in all of the NASTRAN responses and is the reason for removal of the control derivative for this mode from the model. The dominant structural mode in these responses is the first mode identified previously.

Costs for each input/output pair are given in Table 7. Overall, the average cost of  $J_{ave} = 67$  is reduced as compared to the single mode model, indicating excellent agreement that is again well within the recommended guidelines and consistent with the plotted results. Larger costs for the  $p_{IR}/ail$  (Fig. 6(a)) and  $r_{IR}/rud$  (Fig. 7(b)) responses are predominantly due to phase differences between the identified and NASTRAN models at frequencies above the second structural mode. Higher frequency structural modes which are not included in the identification may impact the phase response, giving the larger error.

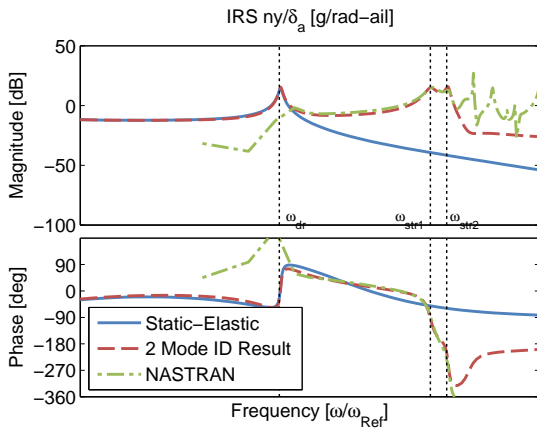
The final identified model Cramer-Rao values and insensitivities of the parameters are shown in Table 8. The second structural mode is dominated by roll motion and so the  $\eta_{p2}$  rigid-body coupling term was the only one with acceptable insensitivity and was retained. The remaining rigid-body coupling derivatives for the model were insensitive and were therefore dropped from the identification. Since the mode does not appear in rudder responses the rudder control derivative was removed. The mode's aileron control derivative was fixed at unity as before in order to remove correlation between the control derivative and the influence coefficients. The final model again shows low insensitivities and high accuracy for all the parameters, indicating a very reliable model. The rigid-body coupling parametric  $\eta_{p2}$  has a slightly elevated Cramer-Rao bound, but the overall identification is still within guidelines since it is the only parameter that is elevated.



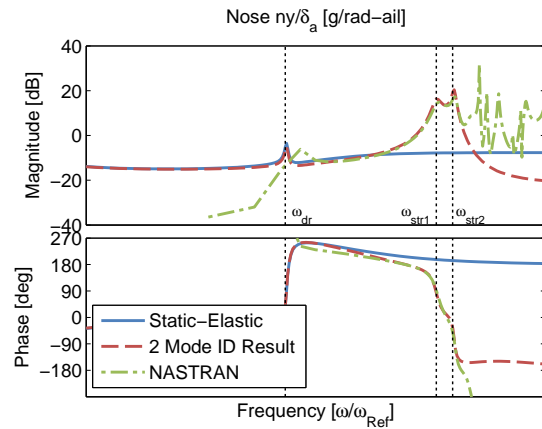
(a) Roll rate response at the IRS sensor



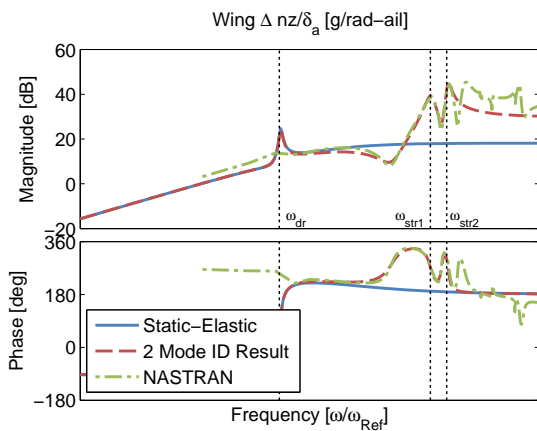
(b) Yaw rate response at the IRS sensor



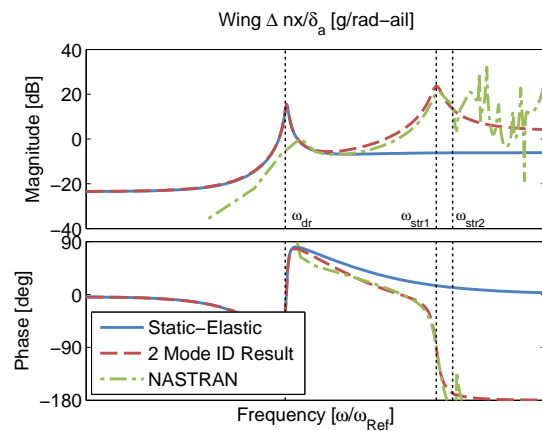
(c) Lateral acceleration response at the IRS sensor



(d) Lateral acceleration response at the nose

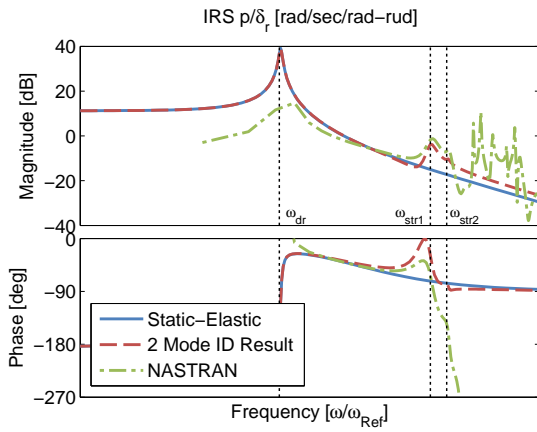


(e) Differential wing tip vertical acceleration response

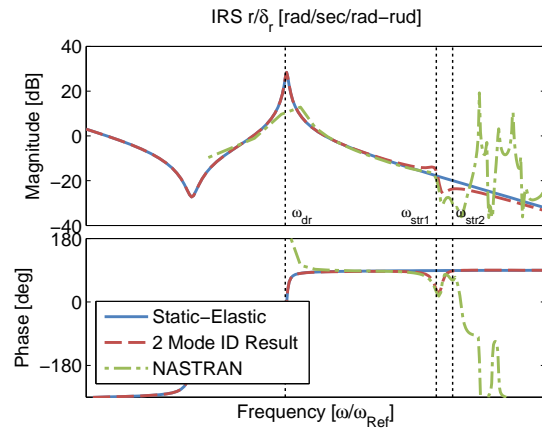


(f) Differential wing tip fore/aft acceleration response

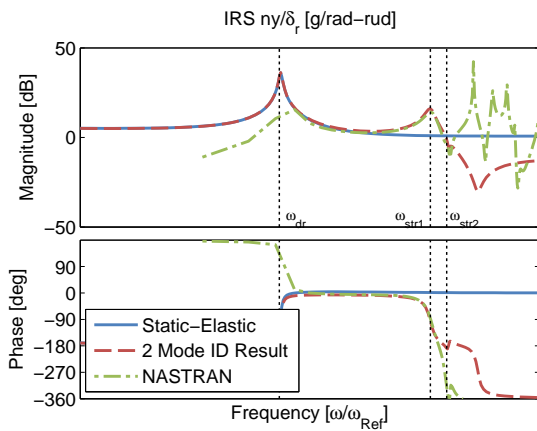
Figure 6. Identified nominal model results for aileron inputs including two structural modes



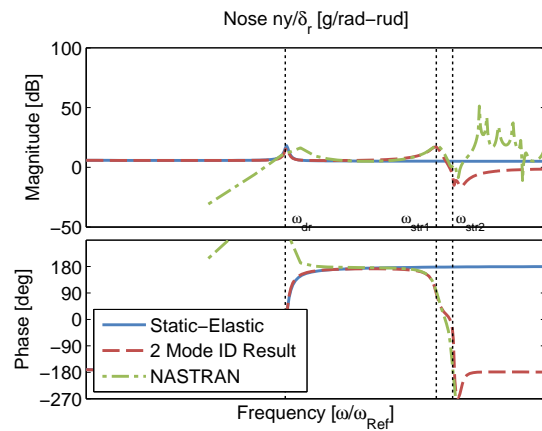
(a) Roll rate response at the IRS sensor



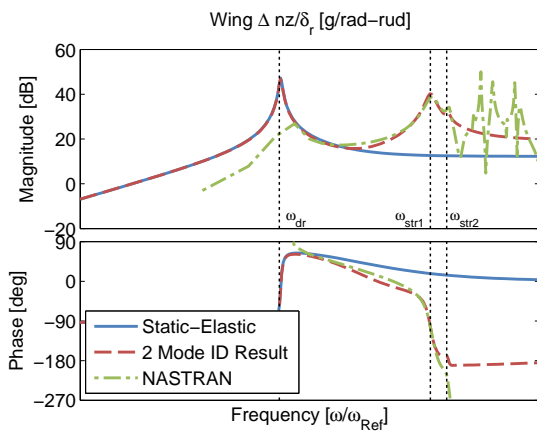
(b) Yaw rate response at the IRS sensor



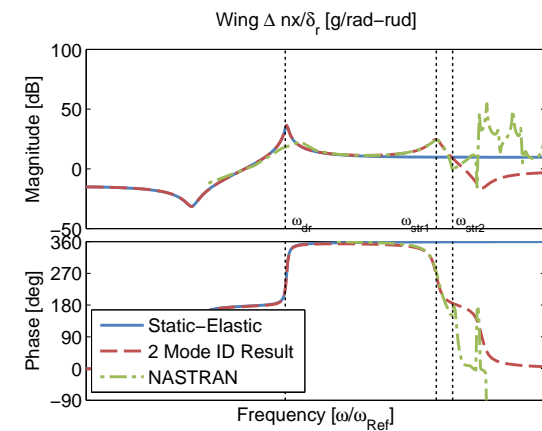
(c) Lateral acceleration response at the IRS sensor



(d) Lateral acceleration response at the nose



(e) Differential wing tip vertical acceleration response



(f) Differential wing tip fore/aft acceleration response

Figure 7. Identified nominal model results for rudder inputs including two structural modes

Table 7. Identification Costs of Two Structural Mode Model

Response	Cost
$pIR/ail$	157.7
$nyIR/ail$	100.9
$nyNs/ail$	50.04
$nzDW/ail$	54.42
$rIR/rud$	108.5
$nyIR/rud$	24.49
$nyNs/rud$	46.9
$nzDW/rud$	44.82
$nxDW/rud$	10.96
$J_{ave}$	66.51

Table 8. Cramer-Rao and Insensitivity Values for Identification of Two Structural Modes

Engineering Symbol	CR (%)	Insens. (%)
$\eta_{v1}^b$	—	—
$\eta_{p1}^b$	—	—
$\eta_{r1}$	9.302	3.798
$2\zeta_{str1}\omega_{str1}$	3.787	1.463
$\omega_{str1}^2$	0.4781	0.1975
$\eta_{\delta_{ail1}}^a$	—	—
$\eta_{\delta_{rud1}}$	3.77	1.177
$\eta_{v2}^b$	—	—
$\eta_{p2}$	26.18	11.27
$\eta_{r2}^b$	—	—
$2\zeta_{str2}\omega_{str2}$	7.708	3.337
$\omega_{str2}^2$	0.4624	0.1896
$\eta_{\delta_{ail2}}^a$	—	—
$\eta_{\delta_{rud2}}^b$	—	—
$\Phi_{pIRS1}$	8.329	3.932
$\Phi_{pIRS2}$	6.316	2.972
$\Phi_{rIRS1}$	7.774	3.323
$\Phi_{rIRS2}^b$	—	—
$\Phi_{nyIRS1}$	4.015	1.668
$\Phi_{nyIRS2}$	7.148	3.171
$\Phi_{nyNose1}$	3.91	1.63
$\Phi_{nyNose2}$	7.47	3.406
$\Phi_{nyTail1}^b$	—	—
$\Phi_{nyTail2}^b$	—	—
$\Phi_{\Delta n_{zw}1}$	3.099	1.243
$\Phi_{\Delta n_{zw}2}$	5.569	2.531
$\Phi_{\Delta n_{xw}1}$	6.339	2.531
$\Phi_{\Delta n_{xw}2}^a$	—	—

<sup>a</sup> Fixed parameter

<sup>b</sup> Eliminated parameter

## VII. Identification of a Hybrid-Flexible Lateral/Directional Model for the Off-Nominal Condition

A hybrid-flexible model with two modes is now identified for the off-nominal flight condition to demonstrate the generality of the method and highlight the changes in model behavior with flight condition. The off-nominal flight condition shown in Fig. 1 has large differences in both the low frequency rigid-body response and the structural response when compared to the nominal case. The same structural modes will be identified as for the nominal flight condition. The nominal model including two structural modes is used to provide an initial guess at the coupling parameters. The structural peaks occur at different frequencies, so the fit range is modified accordingly as shown in Table 9.

**Table 9. Off-Nominal structural mode responses and frequency ranges for model identification including two structural modes**

Output	Input	Response Name	$\omega_{min}$	$\omega_{max}$
$p_{IRS}$	Aileron	$pIR/ail$	10	24
$n_{y_{IRS}}$	Aileron	$ayIR/ail$	10	24
$n_{y_{Nose}}$	Aileron	$ayNs/ail$	10	24
$\Delta n_{zW}^*$	Aileron	$azDW/ail$	10	24
$r_{IRS}$	Rudder	$rIR/rud$	10	18.5
$n_{y_{IRS}}$	Rudder	$ayIR/rud$	10	18.5
$n_{y_{Nose}}$	Rudder	$ayNs/rud$	10	18.5
$\Delta n_{zW}^*$	Rudder	$azDW/rud$	10	18.5
$\Delta n_{xW}^*$	Rudder	$azDW/rud$	10	18.5

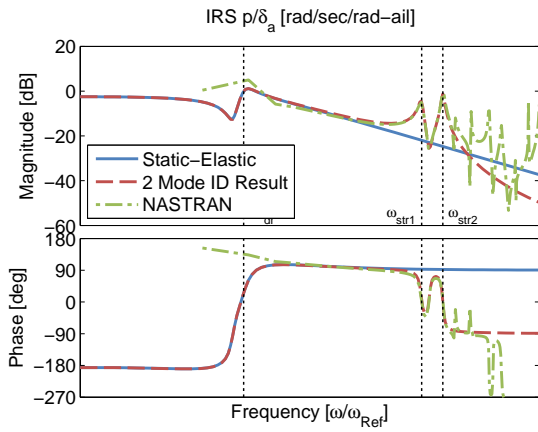
\* Created from differencing individual wing accelerometer measurement, Eqn. (10)

The aileron responses are shown in Fig. 8. Both structural modes are well identified in the dominant roll rate and differential vertical wing tip acceleration responses, Figs. 8(a) and 8(e), respectively. The modes also appear well in the off-axis responses.

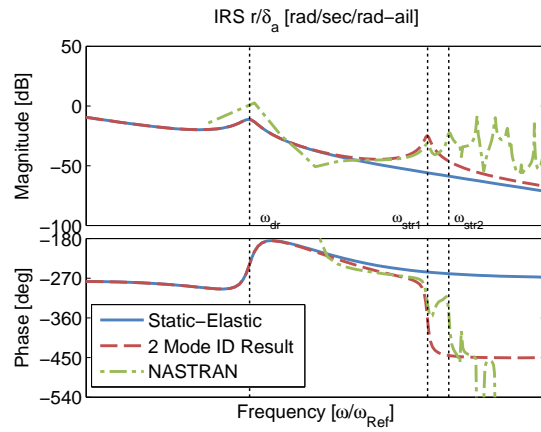
The rudder responses are shown in Fig. 9. As with the nominal case, the lack of excitation of the second mode by the rudder is apparent in all of the NASTRAN responses. The dominant structural mode in these responses is the first mode.

Final costs are shown in Table 10. The overall cost of  $J_{ave} = 30$  is lower than either nominal case, resulting in an excellent identification result. The largest cost is for the lateral acceleration response at the nose to aileron inputs (Fig. 8(d)), which has large coupling to higher frequency modes.

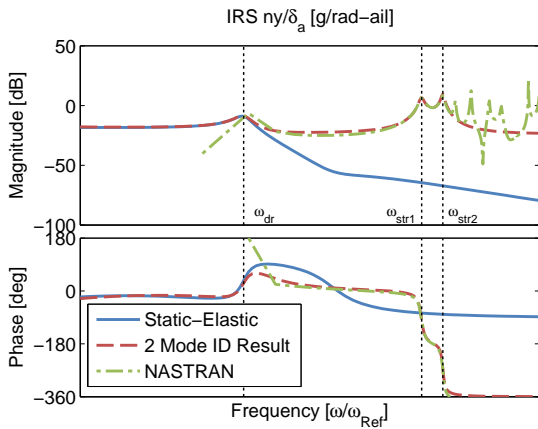
The individual parameter Cramer-Rao and insensitivity values are given in Table 11 and show a reliable model with very low Cramer-Rao and insensitivity values. For the first structural mode, the same coupling exists as for the nominal case. For the second structural mode, all rigid-body coupling parameters were dropped, meaning for the off-nominal loading configuration, the second mode is excited solely by control inputs.



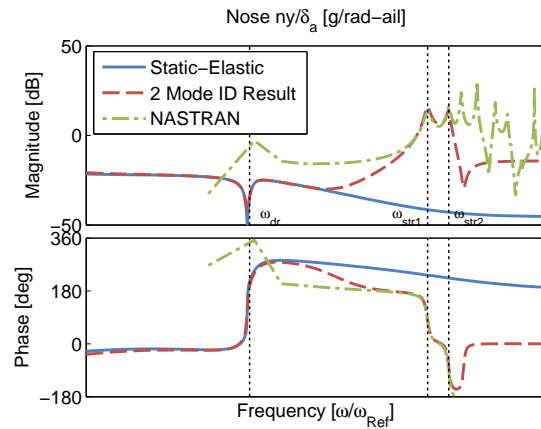
(a) Roll rate response at the IRS sensor



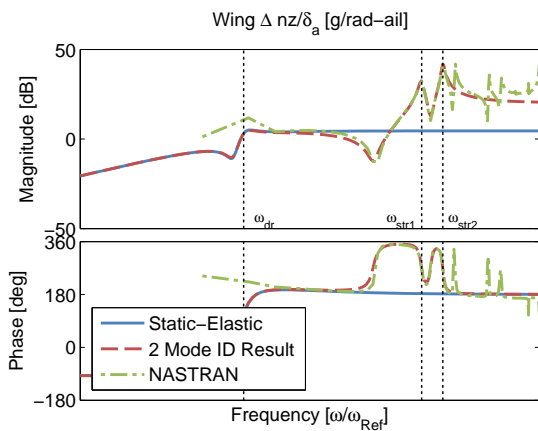
(b) Yaw rate response at the IRS sensor



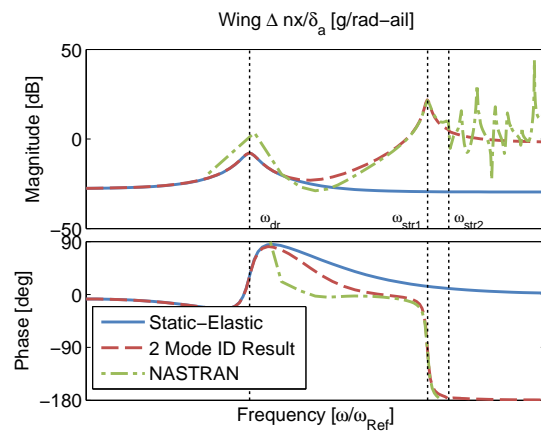
(c) Lateral acceleration response at the IRS sensor



(d) Lateral acceleration response at the nose

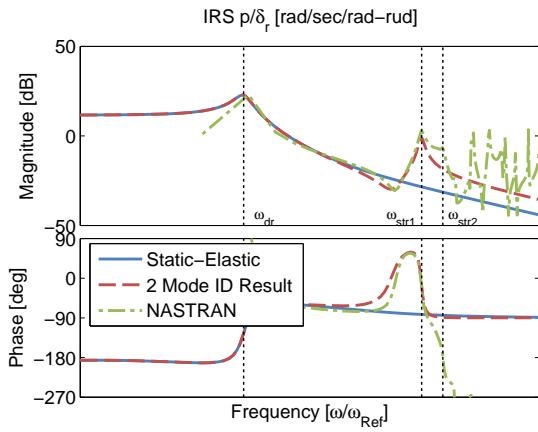


(e) Differential wing tip vertical acceleration response

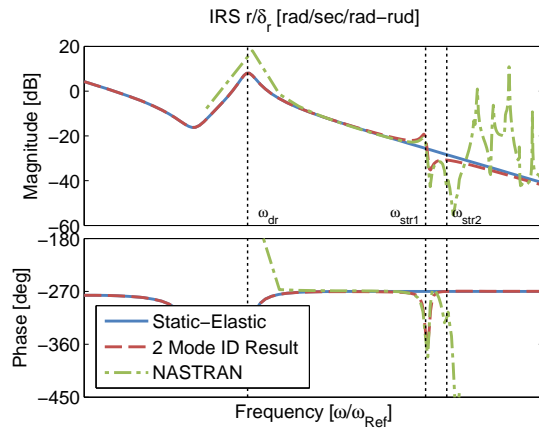


(f) Differential wing tip fore/aft acceleration response

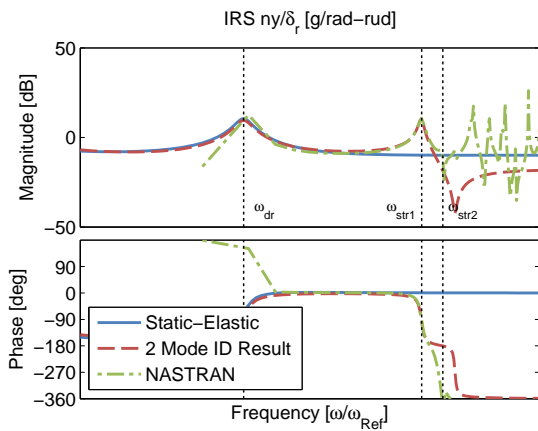
Figure 8. Identified off-nominal model results for aileron inputs including two structural modes



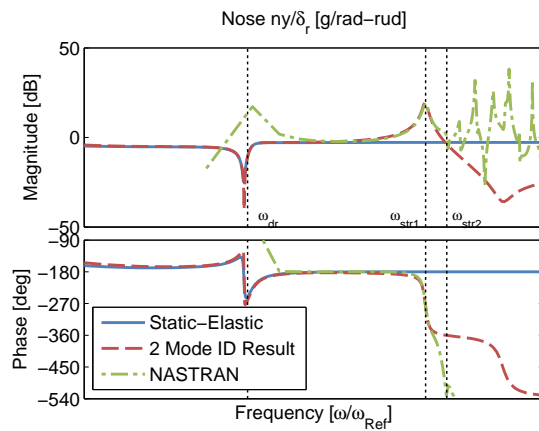
(a) Roll rate response at the IRS sensor



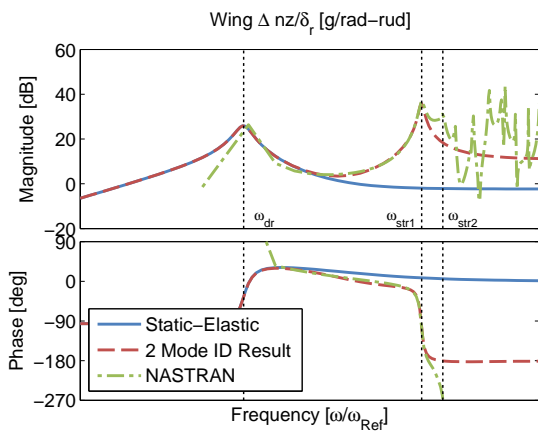
(b) Yaw rate response at the IRS sensor



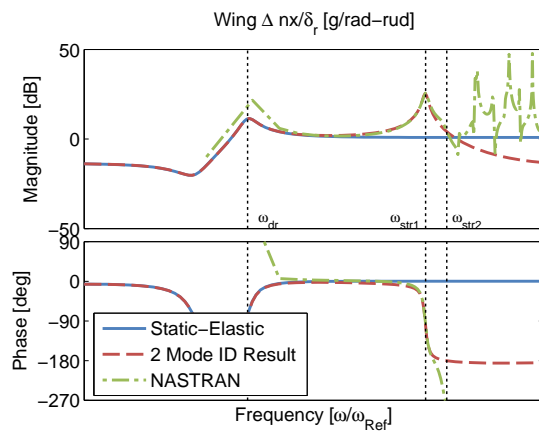
(c) Lateral acceleration response at the IRS sensor



(d) Lateral acceleration response at the nose



(e) Differential wing tip vertical acceleration response



(f) Differential wing tip fore/aft acceleration response

Figure 9. Identified off-nominal model results for rudder inputs including two structural modes

Table 10. Identification of Off-Nominal Model with Two Structural Modes

Response	Cost
$pIR/ail$	18.13
$nyIR/ail$	15.61
$nyNs/ail$	84.94
$nzDW/ail$	13.88
$rIR/rud$	69.07
$nyIR/rud$	14.73
$nyNs/rud$	19.34
$nzDW/rud$	23.86
$nxDW/rud$	12.77
$J_{ave}$	30.26

Table 11. Identification of Off-Nominal Model with Two Structural Modes

Param.	CR (%)	Insens. (%)
$\eta_{v1}^b$	—	—
$\eta_{p1}^b$	—	—
$\eta_{r1}$	15.89	7.215
$2\zeta_{str1}\omega_{str1}$	3.902	1.696
$\omega_{str1}^2$	0.2698	0.1174
$\eta_{\delta_{ail1}}^a$	—	—
$\eta_{\delta_{rud1}}$	3.56	1.085
$\eta_{v2}^b$	—	—
$\eta_{p2}^b$	—	—
$\eta_{r2}^b$	—	—
$2\zeta_{str2}\omega_{str2}$	8.683	3.735
$\omega_{str2}^2$	0.3876	0.1736
$\eta_{\delta_{ail2}}^a$	—	—
$\eta_{\delta_{rud2}}^b$	—	—
$\Phi_{pIRS1}$	4.923	1.993
$\Phi_{pIRS2}$	6.72	2.633
$\Phi_{rIRS1}$	6.469	2.597
$\Phi_{pIRS2}^b$	—	—
$\Phi_{nyIRS1}$	3.795	1.69
$\Phi_{nyIRS2}$	8.959	4.16
$\Phi_{nyNose1}$	3.289	1.465
$\Phi_{nyNose2}$	10.45	4.799
$\Phi_{nyTail1}^b$	—	—
$\Phi_{nyTail2}^b$	—	—
$\Phi_{\Delta n_{zw}1}$	3.111	1.32
$\Phi_{\Delta n_{zw}2}$	3.888	1.756
$\Phi_{\Delta n_{xw}1}$	6.006	2.419
$\Phi_{\Delta n_{xw}2}^a$	—	—

<sup>a</sup> Fixed parameter

<sup>b</sup> Eliminated parameter

## VIII. Flight Control Application

The examples of flight control system design show the importance of a coupled model that includes structural degrees of freedom.

### VIII.A. Generic Notch Filter Design Example

Notch filters are included in flight control systems to attenuate the excitation of structural modes. Typical notch filters are of the form:

$$N(s) = \frac{s^2 + 2\zeta_{\text{num}}\omega_{\text{str}}s + \omega_{\text{str}}^2}{s^2 + 2\zeta_{\text{den}}\omega_{\text{str}}s + \omega_{\text{str}}^2} \quad (20)$$

For low frequency structural modes, the notch filters impact the stability margins in the rigid-body frequency range. To demonstrate this impact, a sample aircraft with a characteristic  $1/s$  broken loop response and a crossover frequency ( $\omega_c$ ) at 3 rad/sec is shown in Fig. 10(a). A rigid aircraft, as well as aircraft with structural modes at 20, 30, and 40 rad/sec are shown. The structural modes themselves do not greatly impact the dynamics around the crossover frequency, but desired gain margins at structural frequencies are not met.

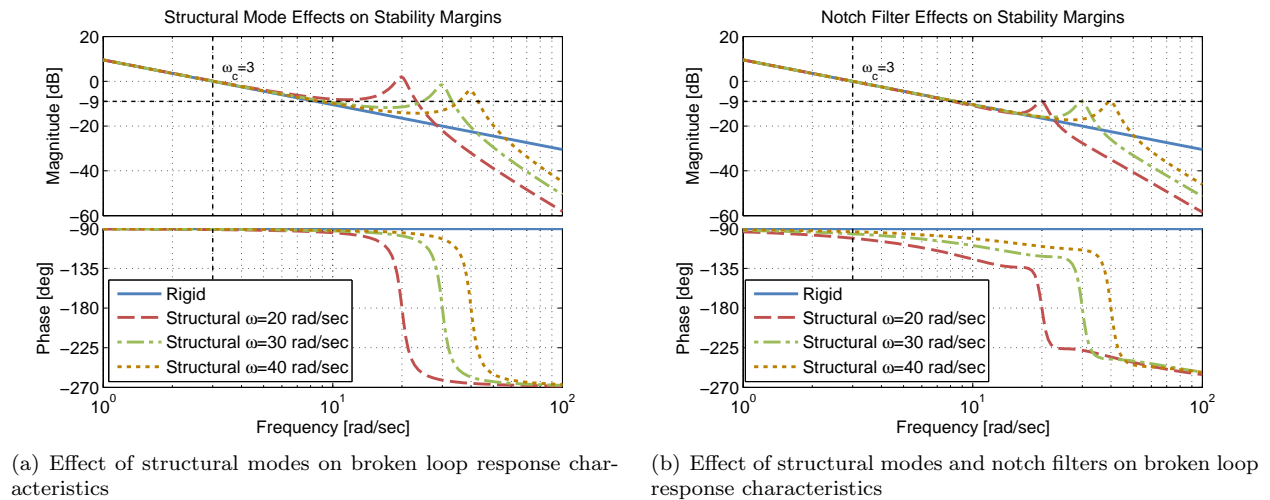


Figure 10. Impact of structural modes on the broken loop response

The structural modes are next attenuated with optimized notch filters to provide exactly 9 dB gain margin at structural frequencies (Fig. 10(b)) as per design standards.<sup>21</sup> If both gain and phase stabilization is used, MIL-DTL-9490E<sup>22</sup> recommends increased gain and phase margins to 8 dB and 60 deg at and above structural frequencies to account for modeling uncertainty.

Table 12 gives the reductions in phase margin at the crossover frequency due to the notch filters. At lower structural frequencies, the structural mode shows up prominently in the broken loop response, and a larger notch filter is needed. This large notch filter has a direct negative impact on the phase response at crossover. At structural frequencies of 20 and 30 rad/sec, the the phase loss is over 5 deg., giving a substantial impact on the control system. At 40 rad/sec, the phase loss is less than 4 deg. The lower the structural mode frequency, the more critical it is to include the mode in the initial compensator design process.

A more generalized design approach applies notch filters with large magnitude attenuation, leading to more phase degradation at crossover than necessary. Using a flexible aircraft model allows for optimal notch filter selection.

This simple example shows that if there are structural modes below 30 rad/sec, they may have a tractable impact on the control system. Inclusion of these modes in a model would be beneficial from a control system design standpoint.

**Table 12. Stability margin degradation due to notch filters in flexible aircraft**

Modal Frequency	Phase Loss at $\omega_c$ (deg)
Rigid	N/A
20 rad/sec	10.8
30 rad/sec	5.9
40 rad/sec	3.5

### VIII.B. Control System Comparisons for the Static-Elastic and Hybrid-Flexible Models

Control system comparisons are given for the nominal static-elastic model and the identified hybrid-flexible model that includes two structural modes. An initial feedback gain set was determined using an LQR methodology based on a selected crossover frequency.<sup>21,23</sup> The feedback measurements available are  $\beta$ ,  $\dot{\beta}$ ,  $\int \beta$ ,  $p$ , and  $\phi$ . This gain set was determined for the static-elastic mode and then applied on the identified hybrid-flexible model. A nominal notch filter is applied on both axes in the hybrid-flexible model to reduce the negative effects of the structural peak on the broken loop response. All responses include actuator dynamics.

The broken loop responses for the lateral and directional axes are shown in Fig 11. The stability margins in the rigid-body frequency range are adequate. However, there are additional peaks at the structural frequencies which significantly impact gain margins. The notch filters reduce these peaks and improve stability.

The Nichols plots of these same responses are shown in Fig. 12. The “exclusion zone” represents combinations of gain and phase margins which are close to the instability point. The phase and gain margin requirements at structural frequencies increase to 60 deg of phase margin and 8 dB of gain margin.<sup>22</sup> Other design requirements may include 9 dB of gain margin over all structural frequencies.<sup>21</sup> These increases account for the increased uncertainty of the response at the structural modes. The structural exclusion zone as well as the -9 dB line are shown in the Nichols margins plots. The traditional static-elastic design gives no impression of reduced stability at structural frequencies. Without the notch filters, the flexible design crosses the exclusion zone and -9 dB line at the structural frequencies, indicating poor stability robustness. When the notch filters are added, the “robustness” of the system is restored and both the exclusion zone and -9 dB crossings are again avoided. The reduction in phase margins due to the notch filters is apparent in the Nichols plots, further motivating the careful notch filter selection available with a flexible aircraft model.

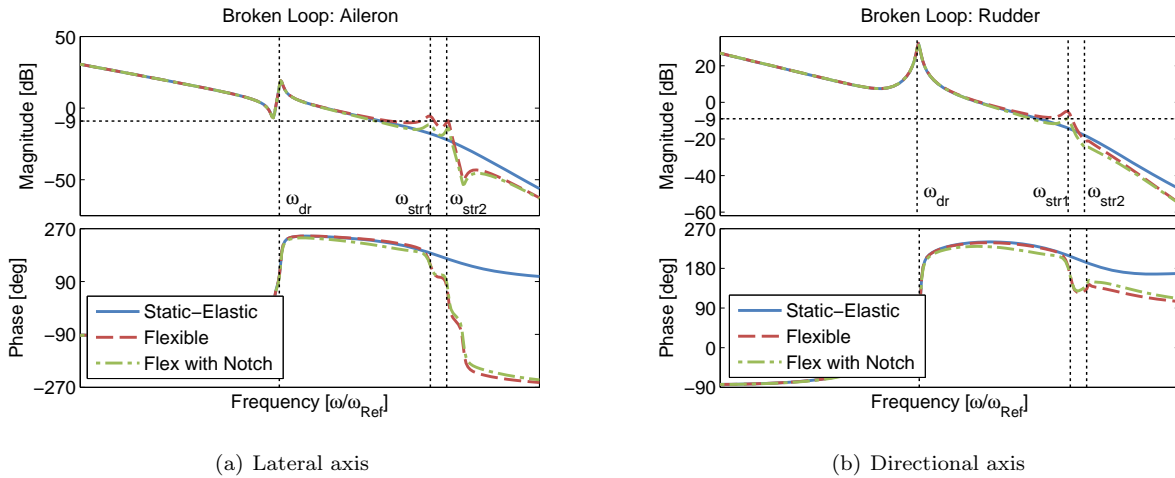


**Figure 11. Broken loop response comparisons**

The loop gain in each axis was varied and the resulting root locus plots are shown in Fig. 13. The static-elastic design for both axes incorrectly predicts large gain margins. Rigid-body feedback signals are

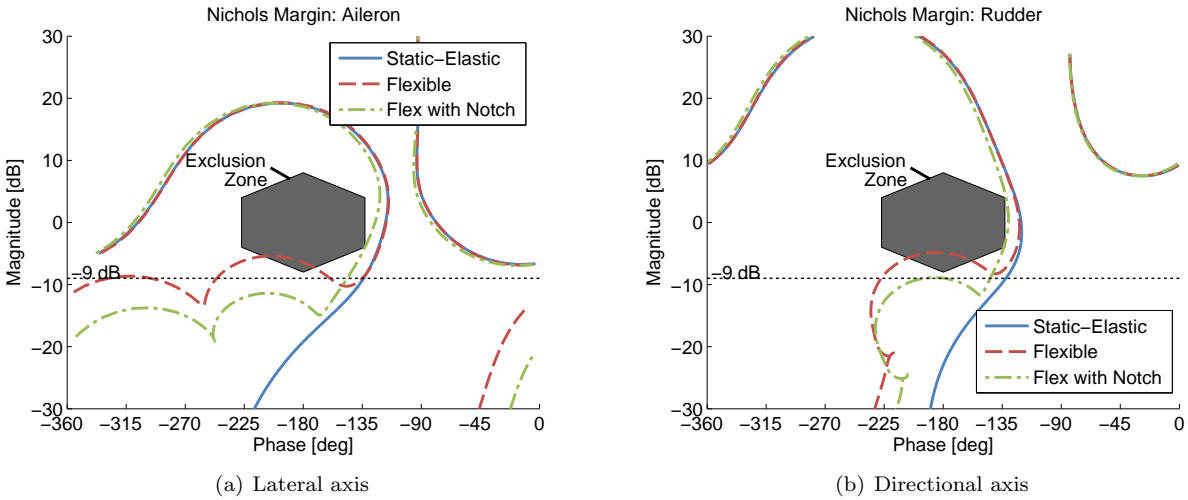


Figure 12. Nichols margin comparisons

seen to be generally destabilizing to structural modes. The flexible system design without notch filters has the lowest gain tolerance before instability is threatened. The notch filters restore larger and acceptable gain margins.

The closed loop responses are shown in Fig. 14. At low frequency all the responses are in close agreement. At the structural frequency, the flexible model has a large excitation peak in both axes. The notch filters reduce this peak as expected. The associate step responses are shown in Fig. 15. The closed loop static-elastic model shows no evidence of the importance structural mode effects. In the lateral axis, there is a large amount of structural oscillation. The notch filter does an excellent job of removing this oscillation. The second structural mode is less excited in the sideslip response to rudder inputs.

## IX. Discussion

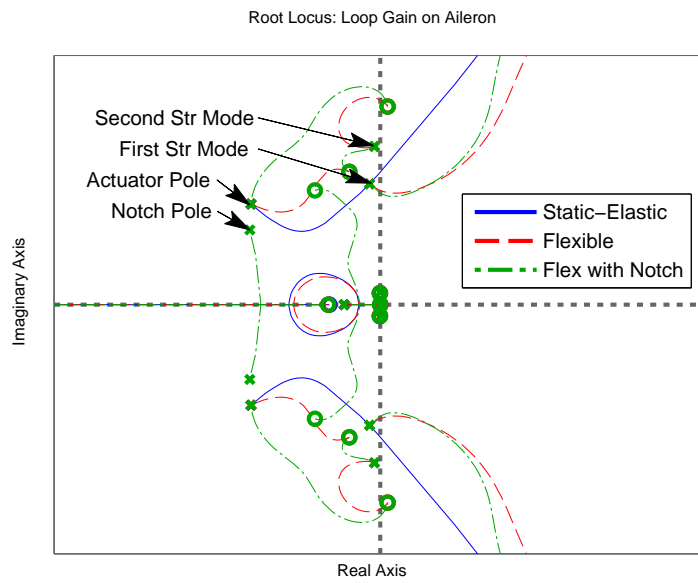
Structural modes and notch filters below 30 rad/sec can impact the dynamics around the crossover frequency and should be included in control system design. A state-space flight dynamics model that is valid over a broad frequency range was identified by combining a static-elastic model and a finite-element NASTRAN structural model. The identification strategy used a hybrid-flexible model structure where there is one way coupling from the rigid-body states to the structural states. Two structural modes were included in the identified model up to a frequency of 30 rad/sec. The static-elastic dynamics are accurate at the rigid-body frequencies and the finite-element NASTRAN model is accurate at the structural frequencies.

The identified model's low parameter insensitivity and Cramer-Rao percentages indicate the parameters were identified accurately. A low average cost for the frequency response comparisons indicates that the identified model behavior is accurate.

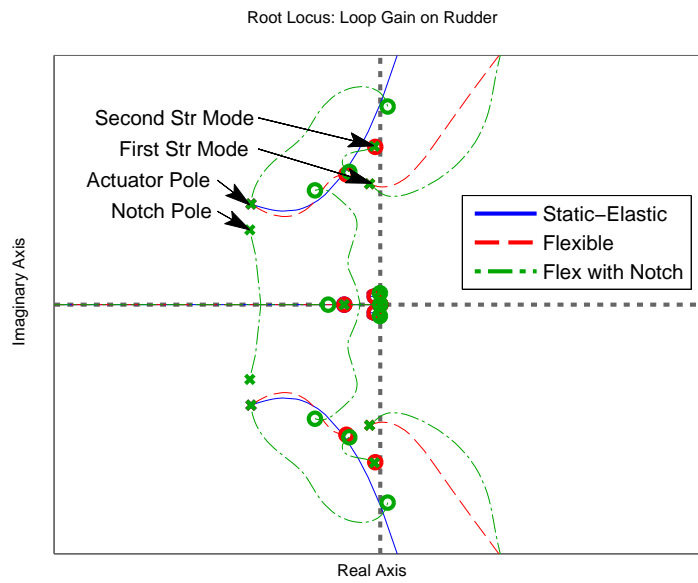
The identification presented uses design models for both the rigid-body and structural dynamics. As more accurate models based on flight data become available, they can easily be substituted and the fidelity of the identified model can be increased. The approach presented is general and not limited to be used with any specific type of model.

A notional LQR control system was implemented to show the capability of the flexible model. With a parametric aircraft representation, root locus and Nichols plots show the influence of the structural modes on the control system response and can help in determining an optimal notch filter compensator with minimal phase degradation. Conventional control system synthesis leads to retuning of the control gains after first flight when an accurate aircraft model that includes structural effects is finally obtained. This iterative nature is costly and inefficient and having an accurate representation of aircraft dynamics can reduce the time required to tune the gains.

There are many applications for the identified flexible aircraft model. For example, load limiting control laws, or control laws that improve ride-quality in turbulence could be implemented.<sup>7</sup> Since the model is valid for a larger frequency range, higher bandwidth (performance) control systems may be developed accurately.

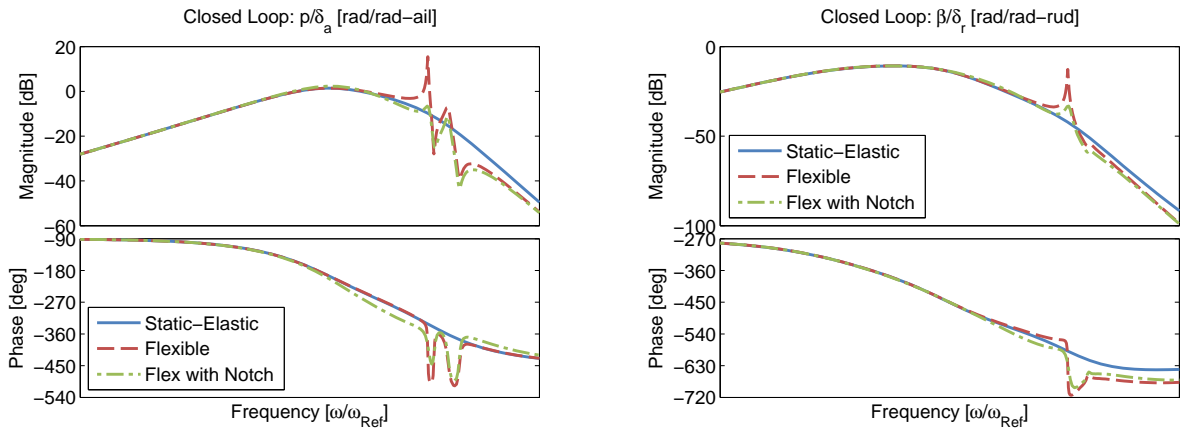


(a) Lateral axis loop gain



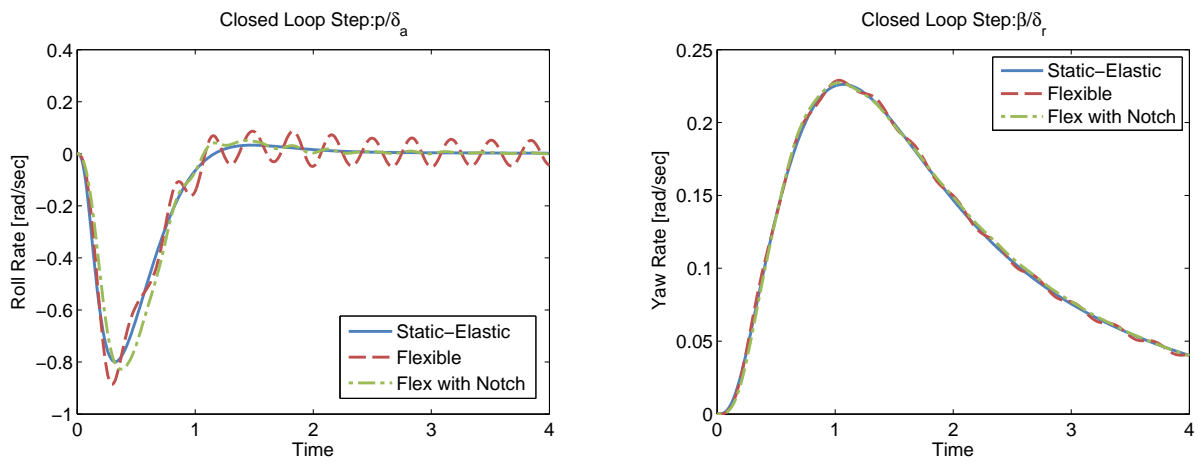
(b) Directional axis loop gain

Figure 13. Root locus plots comparing loop gains on feedback signals



(a) Lateral closed loop roll rate response to aileron inputs (b) Directional closed sideslip response to rudder inputs

Figure 14. Closed loop frequency response comparisons



(a) Lateral closed loop roll rate response to aileron inputs (b) Directional closed sideslip response to rudder inputs

Figure 15. Closed loop step response comparisons

Sensitivity studies on the location of the aircraft sensor package may also be performed to determine the optimal location for the sensors.

## X. Conclusions

Based on the work presented the following conclusions can be drawn:

1. A higher-order aircraft lateral/directional model of a business jet that is accurate up to 30 rad/sec was developed using frequency-domain system identification techniques. This model combines quasi-static stability and control derivatives from a wind-tunnel tuned flight dynamics model with the first two structural modes as obtained from a NASTRAN model.
2. The hybrid-flexible model structure is well suited for system identification of flexible aircraft systems. This model structure was identified for a nominal and off-nominal flight condition to show the general applicability of the method developed. The required measurements for the identification are the aerodynamic control inputs, inertial measurements, and accelerometer measurements at the wing tips, nose, and tail.
3. Control system stability and closed-loop behavior of a business jet is strongly affected by the presence of the lower-frequency structural modes, and these must be included in the design process. Optimal design of notch filters can help reduce phase loss and improve system performance and can only be achieved by using a model that accurately includes the structural modes.

## Acknowledgments

The authors would like to thank Mr. Tom Berger for help with the LQR control design portion of this paper.

## References

- <sup>1</sup>Tischler, M. B. and Remple, R. K., *Aircraft and Rotorcraft System Identification: Engineering Methods with Flight Test Examples*, AIAA, 2nd ed., 2012, Reston, VA.
- <sup>2</sup>Acree, C. W. and Tischler, M. B., "Determining XV-15 Aeroelastic Modes from Flight Data with Frequency-Domain Methods," NASA/TP 3330, May 1993.
- <sup>3</sup>Najmabadi, K., Fritchman, B., and Tran, C., "A Process for Model Identification and Validation of Dynamical Equations for a Flexible Transport Aircraft," RTO SCI Symposium on 'System Identification for Integrated Aircraft Development and Flight Testing', May 1998, Madrid, Spain.
- <sup>4</sup>Theodore, C. R., Ivler, C. M., Tischler, M. B., Field, E. J., Neville, R. L., and Ross, H. P., "System Identification of Large Flexible Transport Aircraft," AIAA Atmospheric Flight Mechanics Conference and Exhibit, August 2008, Honolulu, HI.
- <sup>5</sup>de Oliveira Silva, B. G., "Data Gathering and Preliminary Results of the System Identification of a Flexible Aircraft Model," AIAA Atmospheric Flight Mechanics Conference, August 2011, Portland, OR.
- <sup>6</sup>de Oliveira Silva, B. G. and Mönnich, W., "System Identification of Flexible Aircraft in Time Domain," AIAA Atmospheric Flight Mechanics Conference, August 2012, Minneapolis, MN.
- <sup>7</sup>Kubica, F., "New Flight Control Laws for Large Capacity Aircraft Experimentation on Airbus A340," 21st ICAS Conference, September 1998, Melbourne, Australia.
- <sup>8</sup>LeGarrec, C. and Humbert, M. L., "Identification of the Aeroelastic Model of a Large Transport Civil Aircraft for Control Law Design and Validation," 22nd ICAS Conference, August-September 2000, Harrogate, UK.
- <sup>9</sup>Juhasz, O., Ivler, C. M., Tischler, M. B., and Celi, R., "Control of a Large Flexible Tiltrotor Aircraft," American Helicopter Society Handling Qualities Specialists' Meeting, February 2014, Huntsville, AL.
- <sup>10</sup>Wykes, J. H., Klepl, M. J., and Brosnan, M. J., "Flight Test and Analyses of the B-1 Structural Mode Control System at Supersonic Flight Conditions," NASA CR 170405, December 1983.
- <sup>11</sup>Schmidt, D. K., *Modern Flight Dynamics*, McGraw Hill, 2012, New York, NY.
- <sup>12</sup>Waszak, M. R. and Schmidt, D. K., "Flight Dynamics of Aeroelastic Vehicles," *Journal of Aircraft*, Vol. 25, No. 6, June 1988.
- <sup>13</sup>Meirovitch, L. and Tuzcu, I., "Integrated Approach to the Dynamics and Control of Maneuvering Flexible Aircraft," NASA CR 211748, 2003.
- <sup>14</sup>Juhasz, O., Celi, R., Ivler, C. M., Tischler, M. B., and Berger, T., "Flight Dynamic Simulation Modeling of Large Flexible Tiltrotor Aircraft," American Helicopter Society 68th Annual Forum, May 2012, Fort Worth, TX.
- <sup>15</sup>Sahasrabudhe, V., Faynberg, A., Pozdin, M., Cheng, R., Tischler, M. B., Stumm, A., and Lavin, M., "Balancing CH-53K Handling Qualities and Stability Margin requirements in the Presence of Heavy External Loads," American Helicopter Society 63rd Annual Forum, May 2007, Virginia Beach, VA.

- <sup>16</sup>Juhasz, O., *Flight Dynamics Simulation Modeling and Control of a Large Flexible Tiltrotor Aircraft*, Ph.D. thesis, Department of Aerospace Engineering, University of Maryland, College Park, MD, 2014.
- <sup>17</sup>Duke, E. L., Antoniewicz, R. F., and Krambeer, K. D., "Derivation and Definition of a Linear Aircraft Model," NASA/RP 1207, August 1988.
- <sup>18</sup>Panza, J. L. and Suci, E. O., "In Support of the Stick Model," Aerospace Flutter and Dynamics Council Fall Meeting, October 2005, Wichita, KS.
- <sup>19</sup>Albano, E. and Rodden, W. P., "A Doublet-Lattice Method for Calculating Lift Distributions of Oscillating Surfaces in Subsonic Flows," *AIAA Journal*, Vol. 7, No. 2, February 1969.
- <sup>20</sup>Rodden, W. and Johnson, E., *MSC/NASTRAN Aeroelastic Analysis: User's Guide, Version 68*, MacNeal-Schwendler Corporation, 1994.
- <sup>21</sup>Gangsaas, D., Hodgkinson, J., Harden, C., Saeed, N., and Chen, K., "Multidisciplinary Control Law Design and Flight Test Demonstration on a Business Jet," AIAA Guidance, Navigation, and Control Conference and Exhibit, August 2008, Honolulu, HI.
- <sup>22</sup>Anonymous, "Flight Control Systems - Design, Installation, and Test of Piloted Aircraft, General Specifications for," MIL-DTL-9490E, Department of Defense Interface Standard, February 2006.
- <sup>23</sup>Berger, T., Tischler, M. B., Hagerott, S. G., Gangsaas, D., and Saeed, N., "Lateral/Directional Control Law Design and Handling Qualities Optimization for a Business Jet Flight Control System," AIAA Atmospheric Flight Mechanics Conference, August 2013, Boston, MA.